

TRANSIENT NUMERICAL ANALYSIS OF A HIGH SWIRLED DIESEL ENGINE

Mirko Baratta, mirko.baratta@polito.it
Andrea E Catania, andrea.catania@polito.it
Francesco C Pesce, francesco.pesce@polito.it
Ezio Spessa, ezio.spessa@polito.it
IC Engines Advanced Laboratory, Politecnico di Torino, Italy

Charles Rech, charlesrech@uol.com.br
Flavio V Zancanaro Jr, flavio.zancanaro@ufrgs.br
Horácio A Vielmo, vielmoh@mecanica.ufrgs.br
Mechanical Engineering Department, Federal University of Rio Grande do Sul, Brazil

Abstract. *This paper focuses on a transient cold flow that occurs in a Diesel engine intake, cylinder and exhaust systems. The engine under consideration has a bore of 79.5 mm and a stroke of 86 mm. Numerical solutions using a commercial Finite Volumes CFD code are performed, regarding the velocity and pressure fields, as far as the total air mass discharge and swirl coefficient. Regarding the turbulence, computations were performed with the Reynolds-Averaged Navier-Stokes, Eddy Viscosity Model $k-\omega$ SST, and standard wall functions as near wall treatment. For analysis and comparison, it was applied also the $k-\epsilon$ standard cubic Model (usual in the automotive industry), both in High-Reynolds approach. A moving hexahedral trimmed mesh independence study was performed. In the same way many convergence tests were performed, and a secure criterion established. The enthalpy equation is also solved, and the air compressibility is considered, being treated as a perfect gas. Thought the results it is possible to note divergences between the turbulence models employed.*

Keywords: *Diesel engine, cold transient compressible flow, CFD, moving mesh, turbulence models*

1. INTRODUCTION

The detailed understanding of the flow dynamics characteristics of intake, cylinder and exhaust flow of ICE (Internal Combustion Engines) is necessary for an efficient combustion process and related emissions to the environment. Its accurate and feasible numerical simulation remains a challenge, especially in the case of transient swirling flows, considering the usual complexity of the geometry, the large turbulence spectra associated with the annular vortical jet after the intake valve, adding the compressible non-isothermal effects.

During the last years more numerical simulations have been done regarding the discharge coefficient (Bianchi *et al.*, 2002; Bianchi and Fontanesi, 2003), focusing on directed intake port types, including comparisons with experimental measurements. An even more challenging situation occurs in the presence of swirl generator inlet ports of ramp helical type, including the determination of the swirl coefficient. With the growing availability of turbulence models and computational resources, many works make comparisons, regarding their capacity to reproduce experimental data and CPU time demanding.

Kaario *et al.* (2003) compared the $k-\epsilon$ RNG turbulence model with the one-equation subgrid scale model, incompressible and isothermal LES approach. This particularized form of the LES model used was able to capture more flow's complex structures than the $k-\epsilon$ RNG model, but remains the CPU large time demand problem.

Keeping the popular $k-\epsilon$ family, some works have analyzed the alternatives for the stress-strain relationship, considering the compressible, non-isothermal, anisotropic effects presents in the ICE three-dimensional flows.

Bianchi *et al.* (2002) compared $k-\epsilon$ linear and nonlinear (quadratic and cubic) eddy viscosity models, concluding that cubic stress-strain relation provided the best agreement with data, for those ICE three-dimensional flows considered. In another work Bianchi and Fontanesi (2003) investigated the High Reynolds and Low Reynolds near wall approaches, both with a cubic relationship between Reynolds stresses and strains. It was concluded that the Low Reynolds approach (boundary layer also discretized by the mesh), although increasing the computational effort, presented more ability to capture the details of the tested ICE intake flow.

An alternative is to use RNG models instead of nonlinear ones, considering its underlying concepts similar to non linear models, but with more objective simplicity. Baratta *et al.* (2003) obtained a better experimental agreement for engine flows modifying the RNG constants, presenting another possibility.

Vielmo et al. (2008) compared the k-ε cubic, in its High-Reynolds and Low-Reynolds approaches, for fixed intake valve lifts steady state situations. Thought the results it was possible to note significant divergences between the turbulence models employed, mainly in the calculated swirl coefficients.

The present paper focuses on a transient numerical analysis of the same Diesel engine (Fiat Research Center, 1982; 1983) analyzed in Vielmo et al. (2008). Looking for more suitable turbulence models, the k-ω SST, in its High-Reynolds approach, and the k-ε standard cubic model, in its compressible and non-isothermal approach, were compared, regarding mainly the swirl coefficient.

2. THE SWIRL COEFFICIENT

The engine under investigation is of a four-stroke compression-ignition engine, containing a swirl generator inlet port of shallow ramp helical type (Fiat Research Center, 1982; Tindal *et al.*; 1982). It is coupled with a seat valve with an inner diameter of 31.5 mm, and outer diameter of 34.5 mm. The outlet port is a conventional one, with a valve of an inner diameter of 26.7 mm, and outer diameter of 29.5 mm. The cylinder bore (B) is 79.5 mm, stroke 86 mm, and compression ratio 18:1. The maximum intake valve lift is 8.1 mm, opening at 355° (5° BTDC) and closing at 595° (55° ABDC). The maximum exhaust valve lift is 8.1 mm, opening at 125° (55° BBDC) and closing at 365° (5° ATDC).

An important ICE parameter is the swirl coefficient (Heywood, 1988 ; Fiat Research Center, 1983) who, for a certain valve lift, I_l , is a relation between the flow's angular momentum with its axial moment. On the hypothesis of rigid body, for the angular velocity ω , and axial average velocity v_m ,

$$I_l = \frac{\omega \frac{B}{2}}{v_m} \quad (1)$$

As the real flow does not acts as a rigid body, realizing the product of the position vector and the velocity vector, and numerically calculating the axial average velocity, the Eq. (1) becomes

$$I_l = \frac{\frac{\int_m (zu - xw) dm}{\int_m r^2 dm} \frac{B}{2}}{\frac{\int_m v dm}{\int_m dm}} \quad (2)$$

where the integrations are made with the velocity components of the flow (u, v, w), for the coordinates (x, y, z), and corresponding radius r . As the swirl movement of the air inside the cylinder varies along its axis, it is necessary to define the section where the measure is done.

In the present work the comparisons between the two turbulence models tested are made trough this coefficients, at a certain number of sections. Details along the flow structure are also analyzed.

3. MATHEMATICAL MODEL

The velocity field is described by the mass and momentum conservation equations (Navier-Stokes), in their transient, compressible form.

In Cartesian tensor notation, according Warsi, 1981, the mass conservation is

$$\frac{\partial \rho}{\partial t} + \frac{\partial}{\partial x_j} (\rho u_j) = 0 \quad (3)$$

and the momentum

$$\frac{\partial \rho u_i}{\partial t} + \frac{\partial}{\partial x_j} (\rho u_j u_i - \tau_{ij}) = -\frac{\partial p}{\partial x_i} + s_i \quad (4)$$

where t is the time; x_i is Cartesian coordinate ($i = 1, 2, 3$); u_i is absolute fluid velocity component in direction x_i ; ρ is density; τ_{ij} is the stress tensor components; s_i is momentum source components, $p = p_s - \rho_0 g_m x_m$ is the piezometric pressure, where p_s is static pressure; ρ_0 is reference density; the g_m are gravitational acceleration components; the x_m are coordinates relative to datum where ρ_0 is defined. Repeated subscripts denote summation. As the fluid is Newtonian, and the flow is turbulent, assuming the ensemble average (equivalent to time averages for steady-state situations), the stress tensor components are, according Hinze, 1975,

$$\tau_{ij} = 2\mu s_{ij} - \frac{2}{3}\mu \frac{\partial u_k}{\partial x_k} \delta_{ij} - \overline{\rho u'_i u'_j} \quad (5)$$

where μ is the molecular viscosity,

$$s_{ij} = \frac{1}{2} \left(\frac{\partial u_i}{\partial x_j} + \frac{\partial u_j}{\partial x_i} \right) \quad (6)$$

and δ_{ij} the "Kronecker delta". The u' are fluctuations about the ensemble average velocity, and overbar denotes the ensemble averaging process. Finally, as the flow is compressible and non-isothermal

$$s_i = g_i (\rho - \rho_0) \quad (7)$$

where g_i is the gravitational acceleration component in x_i direction. Considering the air as an ideal gas

$$\rho = \frac{p}{RT} \quad (8)$$

where R is the universal gas constant and T the absolute temperature.

For the heat transfer problem, the enthalpy equation is also solved. According Jones, 1980,

$$\frac{\partial \rho h}{\partial t} + \frac{\partial}{\partial x_j} (\rho h u_j + F_{h,j}) = \frac{\partial p}{\partial t} + u_j \frac{\partial p}{\partial x_j} + \tau_{ij} \frac{\partial u_i}{\partial x_j} \quad (9)$$

where $h \equiv \bar{c}_p T - c_p^0 T_0$ is the static enthalpy; \bar{c}_p is the mean constant-pressure specific heat at temperature T ; c_p^0 the reference specific heat at temperature T_0 , and $F_{h,j}$ the diffusional energy flux in direction x_j , given by

$$F_{h,j} \equiv -k \frac{\partial T}{\partial x_j} + \overline{\rho u'_j h'} \quad (10)$$

where k is the thermal conductivity.

3.1 Constitutive Relations

The rightmost terms of the Eq. (5) and Eq. (10) represents the additional Reynolds stresses due to turbulent motion. These are linked to the mean velocity field via turbulence models. According Launder and Spalding, 1974, for linear viscosity models

$$-\overline{\rho u'_i u'_j} = \mu_t s_{ij} - \frac{2}{3} \left(\mu_t \frac{\partial u_k}{\partial x_k} + \rho k \right) \delta_{ij} \quad (11)$$

$$\overline{\rho u'_j h'} = -\frac{\mu_t}{\sigma_{h,t}} \frac{\partial h}{\partial x_j} \quad (12)$$

where $k \equiv \frac{\overline{u_i u_i}}{2}$ is the turbulence kinetic energy; μ_t the turbulent viscosity; $\sigma_{h,t}$ the turbulent Prandtl number and

$$s_{ij} = \frac{\partial u_i}{\partial x_j} + \frac{\partial u_j}{\partial x_i} \quad (13)$$

is the mean strain. In the $k - \varepsilon$ turbulence model the turbulent viscosity is linked to k and ε (turbulence dissipation rate) via

$$\mu_t = f_\mu \frac{C_\mu \rho k^2}{\varepsilon} \quad (14)$$

where C_μ is an empirical constant coefficient, and f_μ is the dumping function, defined according the individual model variant. In the cubic model applied in the present work, the Eq. (11) has additional terms, according Shih et al., 1993.

3.2 Governing Equations for the Standard $k - \varepsilon$ Model

For linear and non-linear, incompressible and compressible flows (non-linear cubic, compressible, including buoyancy effects in the present work), according El Tahry, 1983, and Rodi, 1979, for the turbulent kinetic energy

$$\frac{\partial}{\partial t}(\rho k) + \frac{\partial}{\partial x_j} \left[\rho u_j k - \left(\mu + \frac{\mu_t}{\sigma_k} \right) \frac{\partial k}{\partial x_j} \right] = \mu_t (P + P_B) - \rho \varepsilon - \frac{2}{3} \left(\mu_t \frac{\partial u_i}{\partial x_i} + \rho k \right) \frac{\partial u_i}{\partial x_i} + \mu_t P_{NL} \quad (15)$$

where $P \equiv s_{ij} \frac{\partial u_i}{\partial x_j}$; $P_B \equiv -\frac{g_i}{\sigma_{h,t}} \frac{1}{\rho} \frac{\partial \rho}{\partial x_i}$; $P_{NL} = -\frac{\rho}{\mu_t} \overline{u_i u_j} \frac{\partial u_i}{\partial x_j} - \left[P - \frac{2}{3} \left(\frac{\partial u_i}{\partial x_j} + \frac{\rho k}{\mu_t} \right) \frac{\partial u_i}{\partial x_j} \right]$ for non-linear models and σ_k is the turbulent Prandtl number. The first term on the right-hand side of Eq. (15) represents turbulent generation by shear and normal stresses and buoyancy forces, the second viscous dissipation, and the third amplification or attenuation due to compressibility effects. The last term accounts for the non-linear contributions.

For the turbulent dissipation rate

$$\begin{aligned} \frac{\partial}{\partial t}(\rho \varepsilon) + \frac{\partial}{\partial x_j} \left[\rho u_j \varepsilon - \left(\mu + \frac{\mu_t}{\sigma_\varepsilon} \right) \frac{\partial \varepsilon}{\partial x_j} \right] = \\ C_{\varepsilon 1} \frac{\varepsilon}{k} \left[\mu_t P - \frac{2}{3} \left(\mu_t \frac{\partial u_i}{\partial x_i} + \rho k \right) \frac{\partial u_i}{\partial x_i} \right] + C_{\varepsilon 3} \frac{\varepsilon}{k} \mu_t P_B - C_{\varepsilon 2} \rho \frac{\varepsilon^2}{k} + C_{\varepsilon 4} \rho \varepsilon \frac{\partial u_i}{\partial x_i} + C_{\varepsilon 1} \frac{\varepsilon}{k} \mu_t P_{NL} \end{aligned} \quad (16)$$

where σ_ε is the turbulent Prandtl number and the other constants are given in Tab. 1. The first term on the right-hand side of Eq. (16) represents the contribution to the production of dissipation due to linear stresses and dilatation/compression effects. The second term the contribution due to buoyancy, the third accounts for the dissipation destruction, the fourth the contribution due to temporal mean density changes, and the fifth the contribution due to non-linear stresses.

Table 1. Coefficients of the Standard $k - \varepsilon$ Turbulence Model

C_μ	σ_k	σ_ε	σ_h	σ_m	$C_{\varepsilon 1}$	$C_{\varepsilon 2}$	$C_{\varepsilon 3}$	$C_{\varepsilon 4}$	f_μ
0.09	1.0	1.22	0.9	0.9	1.44	1.92	0.0 or 1.44 if $P_B > 0$	-0.33	1.0

3.3 Governing Equations for the SST $k - \omega$ Model

The specific dissipation rate is defined as $\omega = \frac{\varepsilon}{C_\mu k}$, and the general form of the turbulent kinetic energy is

$$\frac{\partial}{\partial t}(\rho k) + \frac{\partial}{\partial x_j} \left[\rho u_j k - \left(\mu + \frac{\mu_t}{\sigma_k^\omega} \right) \frac{\partial k}{\partial x_j} \right] = \mu_t P - \rho \beta^* k \omega + \mu_t P_B \quad (17)$$

and specific dissipation rate is

$$\frac{\partial}{\partial t}(\rho \omega) + \frac{\partial}{\partial x_j} \left[\rho u_j \omega - \left(\mu + \frac{\mu_t}{\sigma_\omega^\omega} \right) \frac{\partial \omega}{\partial x_j} \right] = \alpha \frac{\omega}{k} \mu_t P - \rho \beta \omega^2 + \rho S_\omega + C_{\varepsilon 3} \mu_t P_B C_\mu \omega \quad (18)$$

where $C_{\varepsilon 3}$ and C_μ are empirical coefficients whose default values are given in Tab. 1. For the SST $k - \omega$ model the other coefficients are given in Menter, 1993.

3.4 Boundary and initial conditions

The boundary conditions are stagnation pressure of 1 atm at the inlet, with 293 K, discharging in an ambient pressure of 1.0 atm, and 293 K.

For all cases the turbulence boundary conditions are turbulence intensity $I \equiv \frac{\sqrt{(u')^2}}{U} = 0.05$ (where U is the magnitude of local mean or average velocity on boundary), and length scale $l = 0.0035$ m, as a consequence of the flow and geometrical characteristics.

Regarding the heat transfer problem, considering a cold flow (exhaust and compression processes, without combustion), the cylinder wall and piston crown have a constant temperature of 400 K, and a thermal resistance of 0.004 m²K/W. For the combustion dome 450 K and 0.004 m²K/W. For the admission and exhaust valves and ports 350 K and 0.004 m²K/W.

The initial condition is the crank angle of 320°, what means the end of the exhaust process, followed by the valve crossing and after the air admission. All the velocity components are set 1 m/s, at 1 atm and 300 K. Regarding the turbulence, $k = 0$ for both models applied.

4. NUMERICAL METHODOLOGY

Numerical transient solutions using a commercial Finite Volumes CFD code (StarCD_es-ice, 2008) were performed, regarding the swirl coefficient and the flow structure, for an engine speed of 2000 rpm. An user defined unstructured hexahedral-trimmed cells moving mesh was constructed, as showed in the Fig. 1. In order to provide an adequate capture of the variable gradients, the mesh was refined in the moving valves region, as can be seen in the Fig. 2. A mesh independence study was performed in previous similar works (Vielmo et al., 2008). In this case the mesh has 755788 cells in the cylinder, 212162 in the inlet duct and 149921 in the exhaust.

For the turbulence models applied, k- ε standard cubic and k- ω SST, in its High-Reynolds approach, it was kept $y^+ < 30$. It is important to point that the k- ε standard, although not completely adequate for this case where the stream lines have large curvatures, is very popular in the automotive industry, and by this reason is also applied here.

In the same way many convergence tests were performed, and a secure criterion established. All computations were performed in double precision.

The pressure-velocity coupling is solved thought the SIMPLE algorithm.

By the complexity of the flow, aiming a stable solution, it was necessary to underrelax the momentum with 0.4, pressure 0.2, temperature 0.6, k- ε - ω 0.6, density 0.4, viscosity 0.4.

The time integration was made thought a fully implicit Euler scheme, with a constant time step of 1.1111E-5 s, for a crank angular velocity of 2000 rpm.

The linear algebraic equations system was solved by the method of scalar preconditioned conjugate gradient.

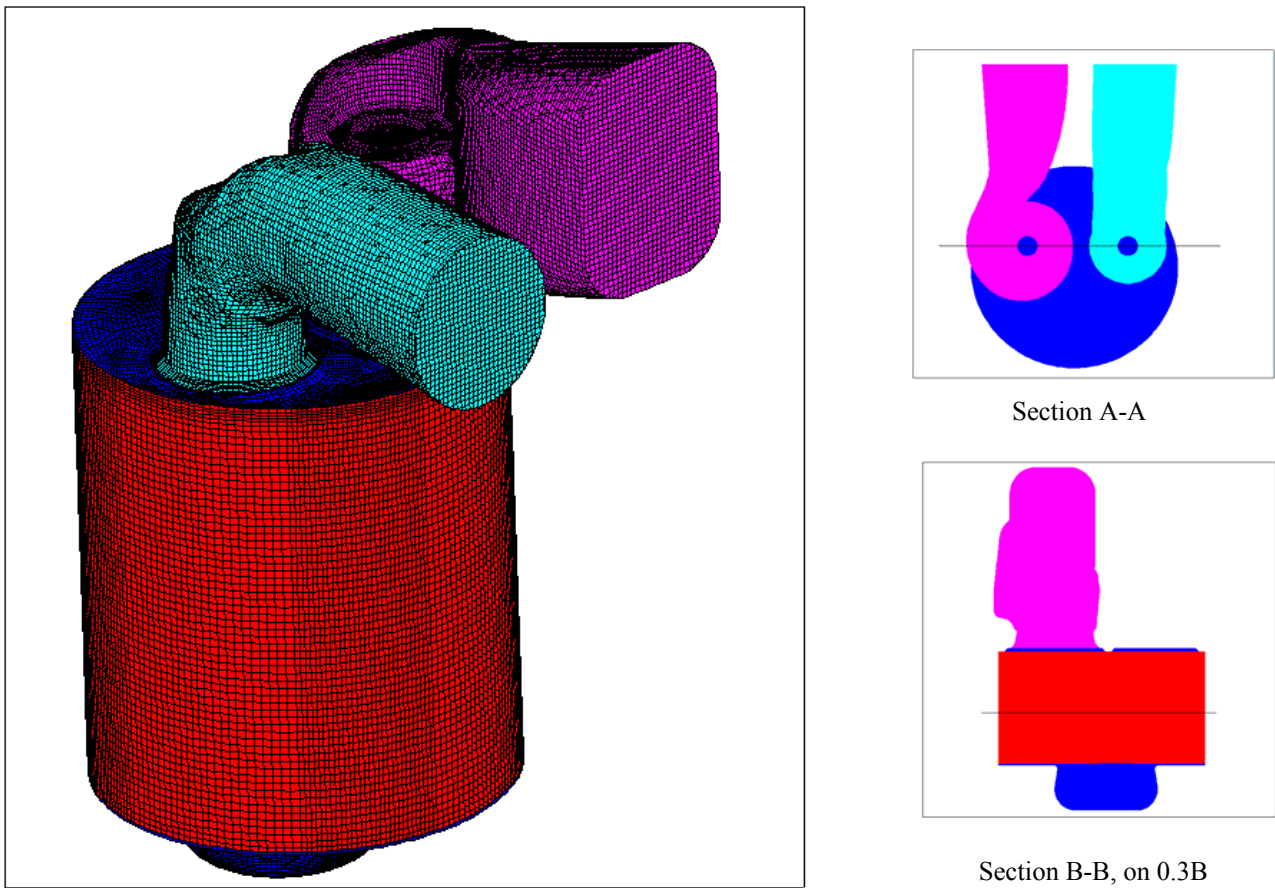


Figure 1. Unstructured hexahedral-trimmed cells moving mesh

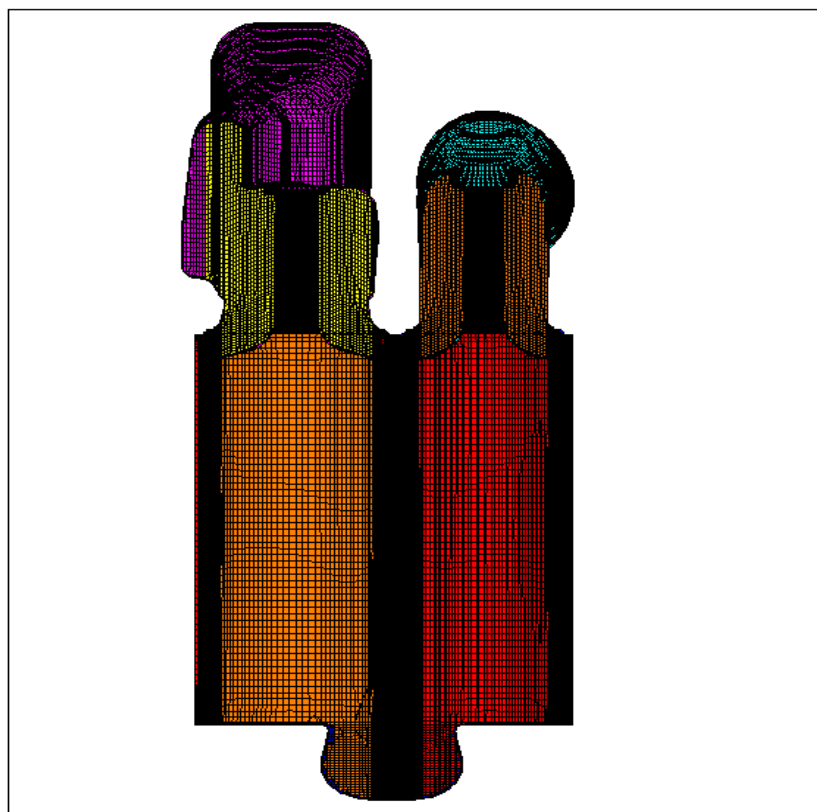


Figure 2. Section A-A mesh detail

4.1 Differencing schemes

As differencing schemes, were applied the Linear Upwind Differencing (LUD), according Wilkes and Thompson, 1983, with blending factor (bf) of 0.3 for the momentum, turbulence and enthalpy equations.

For the density the Central Differencing (CD), according Hirsch, 1960, with bf = 0.3 (StarCD_es-ice User Guides, 2008).

5. RESULTS AND DISCUSSION

In order to compare the results produced by the two turbulence models tested, the following figures show velocity vectors and pressure fields for a crank angle of 444° , close to the maximum piston velocity, where it can be verified the extreme situations, regarding the flow complexity.

The time period, since the initial condition, is $1.0333\text{E-}2$ s, corresponding to an angular interval of 124° ($320^\circ - 444^\circ$).

Two significant sections are showed, being important to point that the unique difference between these solutions is the turbulence model (same boundary and initial conditions, mesh, time step, differencing schemes, etc.).

The intake valve lift in this moment is 7.373 mm.

The Fig. 3 shows that the flow patterns produced by each turbulence model are similar, although the centers of the recirculations do not coincide exactly. It can also be seen that the annular vortical jets caused by the valve have different dimensions and peak velocities (155 m/s for the k- ϵ std and 138.9 m/s for the k- ω SST). The local recirculation at the end of the valve rod – beginning of the valve plane, already detected in previous works (Vielmo et al., 2008, and Rech et al., 2008), is also present.

In the Fig. 4 it is possible to note a crescent divergence between the flow patterns, along its radial dimension and also angularly. In part this is because this figure covers a minor velocity spectrum, becoming the differences more visible.

Focusing the pressure fields, the Fig. 5 shows, as expected, the minimum values near the valve seat (maximum velocities). After this region, the pressure returns increasing to cylinder inside, with a fast transition for the k- ϵ model.

As already seen for the velocity fields, it is possible to see in the Fig. 6 a large variation between the turbulence models when examining the section B-B.

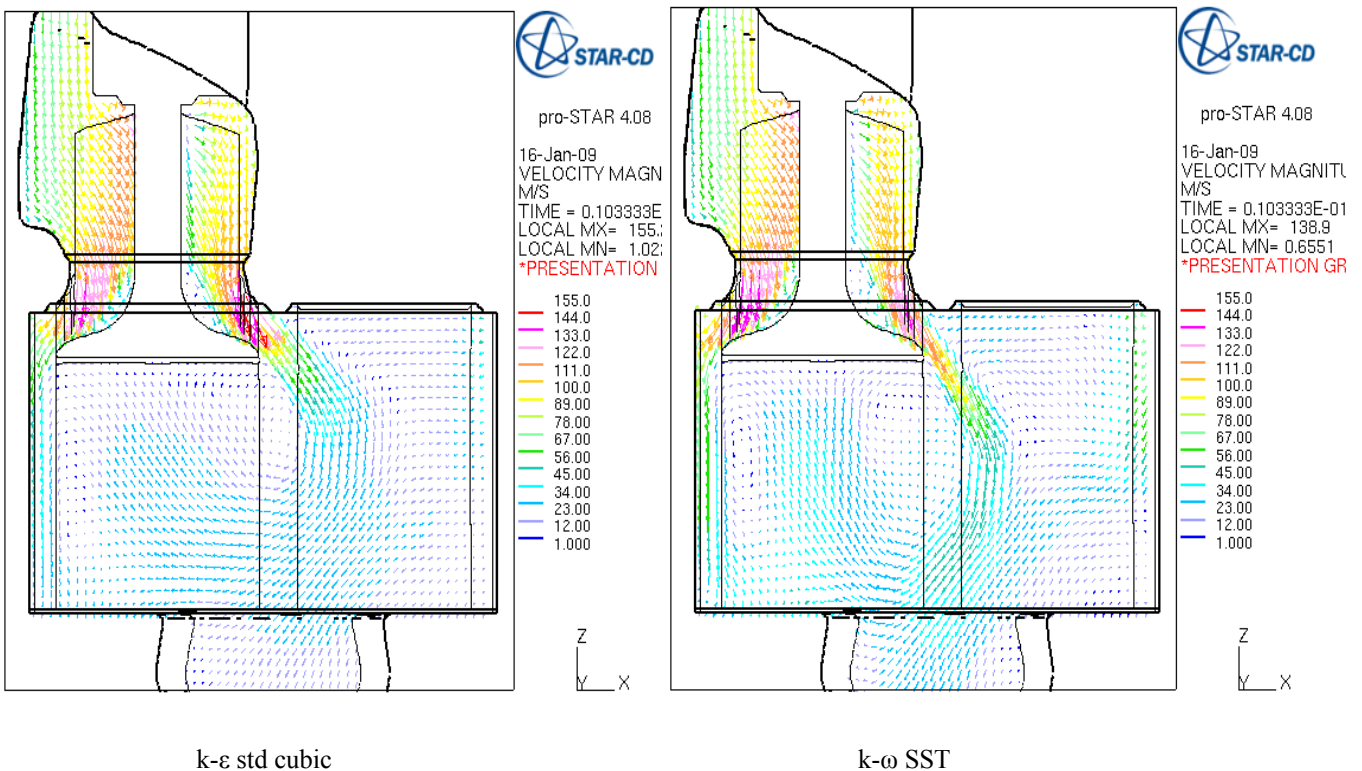


Figure 3. Velocity vectors on section A-A, at 444°

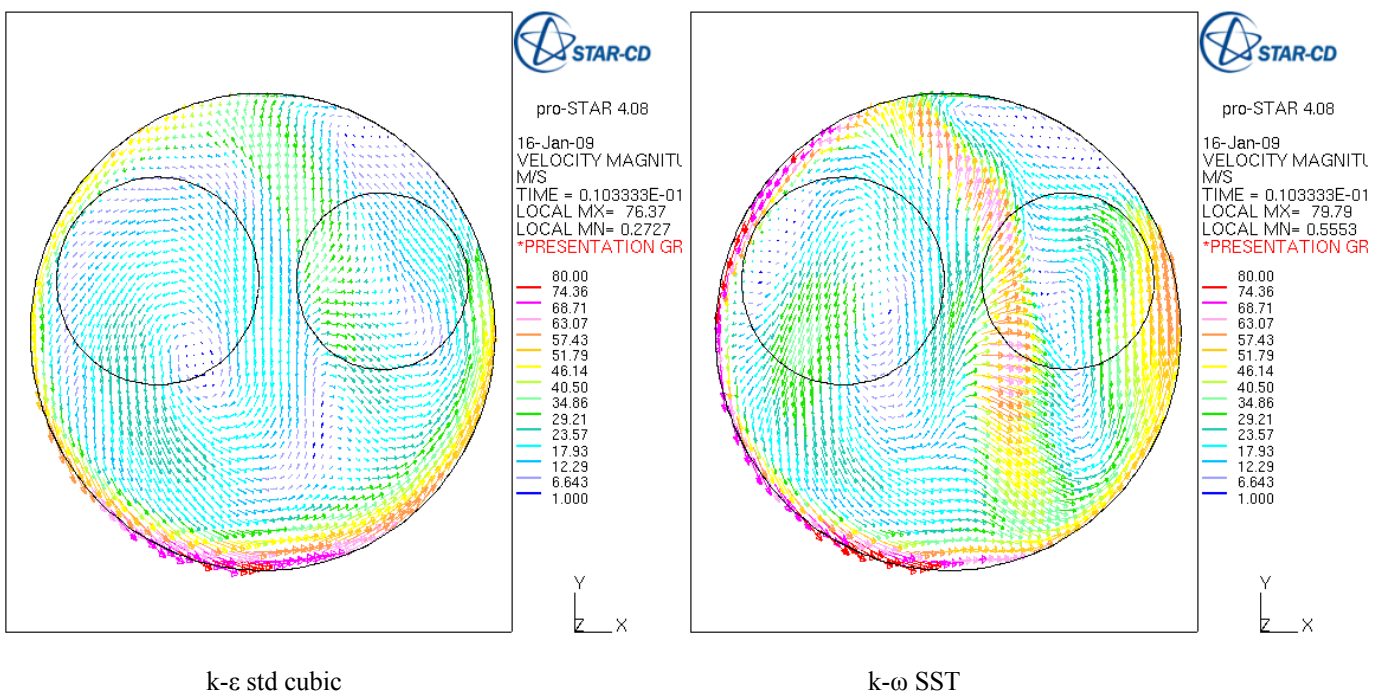


Figure 4. Velocity vectors on section B-B, at 444°

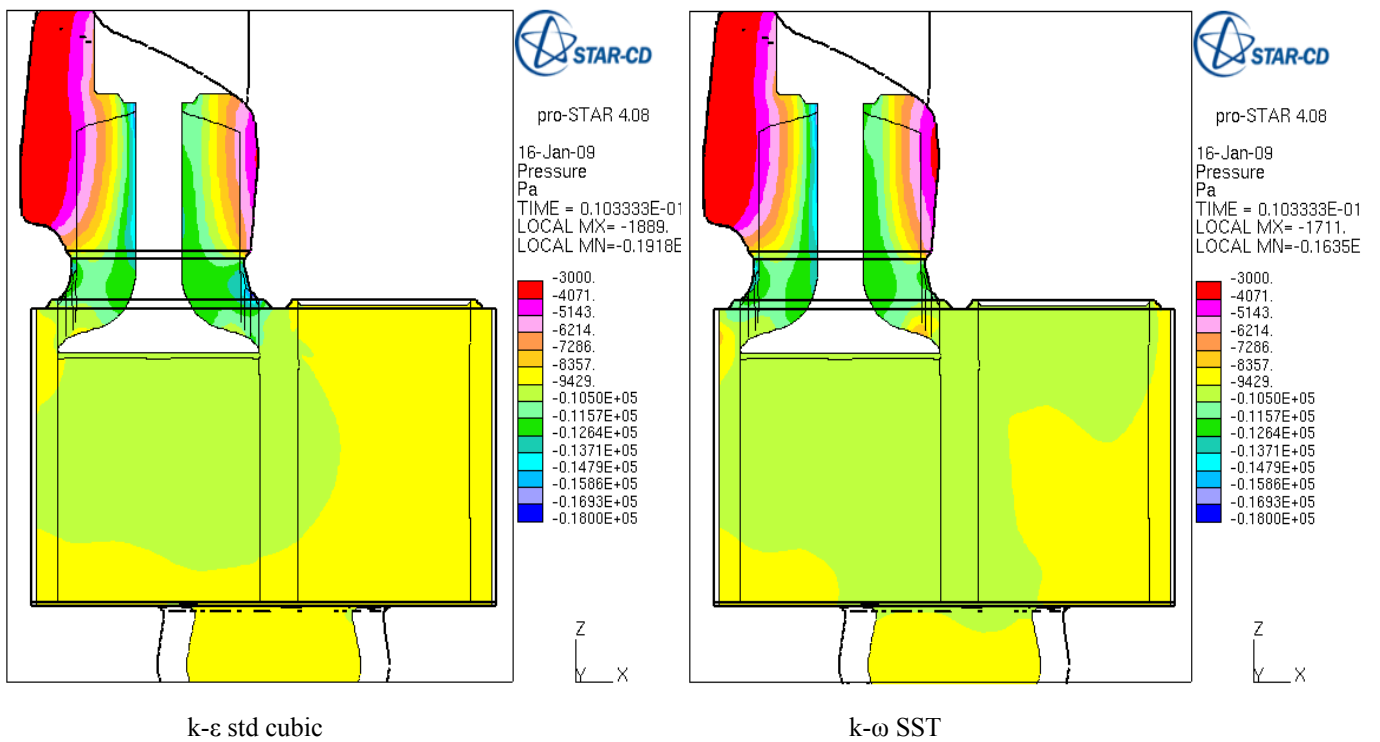


Figure 5. Pressure fields on section A-A, at 444°

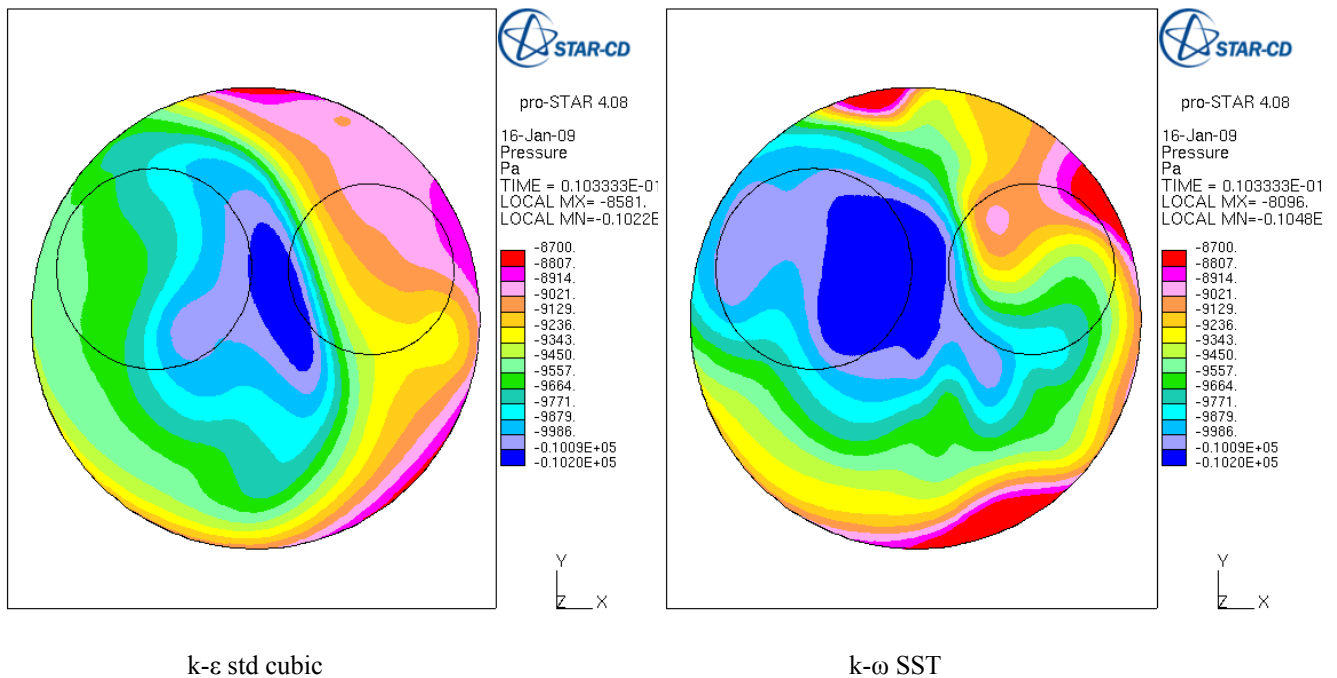


Figure 6. Pressure fields on section B-B, at 444°

Other comparative parameters are presented in the Tab. 2. The air mass discharge (numerically integrated) and the swirl coefficient (Eq. 2) are non local, but global parameters, giving important information about the simulation results. The difference relative to k-ε std cubic model is small for the air mass discharge, but significant for the swirl coefficient.

Table 2. Global comparative parameters at 444°, 7.373 mm intake valve lift

Turbulence model	k-ε std cubic	k-ω SST	Difference relative to k-ε std cubic [%]
Air mass discharge, \dot{m}_l [kg/s]	0.049085	0.048648	-0.90
Swirl coefficient, I_l	3.154	3.496	10.84

6. CONCLUSIONS

Regarding the turbulence, computations were performed with the Reynolds-Averaged Navier-Stokes, Eddy Viscosity Model k-ω SST, and standard wall functions as near wall treatment. For analysis and comparison, it was applied also the k-ε standard cubic Model (usual in the automotive industry), both in High-Reynolds approach.

The comparative parameters presented in the Tab. 1, air mass discharge and swirl coefficient (Eq. 2), show that the difference relative to k-ε std cubic Model is small for the air mass discharge, but significant for the swirl coefficient (10.84 %).

Including the differences observed between the flow patterns, it is possible to conclude that the presented deviations are sufficient to prejudice a detailed project of the engine internal fields, necessary to a correct simulation of reactive flows (combustion).

New searches need to be developed, aiming to clarify the simulation of the turbulence phenomenon in this kind of complex transient, multidimensional, compressible swirling non-isothermal flow, in movable domain.

7. ACKNOWLEDGMENTS

The authors thank the financial support from CAPES through a master scholarship grant to Zancanaro, F.V.Jr.

8. REFERENCES

- Baratta, M., Catania, A.E., Spessa, E., Liu, R.L., 2003. "Multidimensional Predictions of In-Cylinder Turbulent Flows: Contribution to the Assessment of $k-\varepsilon$ Turbulence Model Variants for Bowl-In-Piston Engines". ASME J. of Eng. Gas Turbines Power, 127, pp. 883-896.
- Baratta, M., Catania, A.E., Pesce, F.C., Spessa, E., Vielmo, H.A., 2008. "Numerical Analysis of a High Swirl-Generating Helical Intake Port for Diesel Engines". Proceedings of the 12th Brazilian Congress of Thermal Engineering and Sciences, Belo Horizonte, Brazil.
- Baratta, M., Catania, A.E., Pesce, F.C., Spessa, E., Rech, C., Vielmo, H.A., 2008. "Comparisons Between Steady State Analyses of a High Swirl-Generating Helical Intake Port for Diesel Engines". Proceedings of the 12th Brazilian Congress of Thermal Engineering and Sciences, Belo Horizonte, Brazil.
- Bianchi, G.M., Cantore, G., Fontanesi, S., 2002. "Turbulence Modeling in CFD Simulation of ICE Intake Flows: The Discharge Coefficient Prediction". SAE Paper N° 2002-01-1118.
- Bianchi, G.M., Cantore, G., Parmeggiani, P., Michelassi, V., 2002. "On Application of Nonlinear $k-\varepsilon$ Models for Internal Combustion Engine Flows". Transactions of the ASME vol. 124, pp. 668-677.
- Bianchi, G.M., Fontanesi, S., 2003. "On the Applications of Low-Reynolds Cubic $k-\varepsilon$ Turbulence Models in 3D Simulations of ICE Intake Flows". SAE Paper N° 2003-01-0003.
- El Tahry, S.H., 1983. " $k-\varepsilon$ Equation for Compressible Reciprocating Engine Flows", AIAA J Energy, 7(4), pp. 345-353 Fiat Research Center; Consiglio Nazionale delle Ricerche, 1982. "Motore Monocilindro Diesel con Distribuzione a 2 Valvole e Protezioni Termiche Camera di Combustione". Contract N° 82.00047.93 (in italian).
- Fiat Research Center; Consiglio Nazionale delle Ricerche, 1983. "Metodologia per la Caratterizzazione dei Condotti di Aspirazione Motori in Flusso Stazionario". Contract N° 82.00047.93 (in italian).
- Heywood, J.B., 1988. "Internal Combustion Engines". McGraw-Hill Inc.
- Hinze, P.O., 1975. "Turbulence". 2nd Edition, McGraw-Hill, New York.
- Hirsch, C., 1960. "Numerical Computational of Internal and External Flows – Vol. II: Computational Methods for Inviscid and Viscous Flows". John Wiley & Sons, New York.
- Jones, W.P., 1980. "Prediction Methods for Turbulent Flow". Hemisphere, Washington, D.C., pp. 1-45.
- Kaario, O., Pokela, H., Kjalman, L., Tiainen, J., Larmi, M., 2003. "LES and RNG Turbulence Modeling in DI Diesel Engines". SAE Paper N° 2003-01-1069.
- Launder, B.E. and Spalding, D.B., 1974. "The Numerical Computation of Turbulent Flows". Computational Methods in Applied Mechanics and Engineering, 3, pp. 269-289.
- Menter, F.R., 1993. "Zonal two Equation $k-\omega$ Turbulence Models for Aerodynamic Flows". Proc. 24th Fluid Dynamics Conf., Orlando, Florida, USA, Paper No. AIAA 93-2906.
- Rodi, W., 1979. "Influence of Buoyancy and Rotation on Equations for the Turbulent Length Scale". Proc. 2nd Symp. on Turbulent Shear Flows.
- Shih, T.H., Zhu, J. and Lumley, J.L., 1993. "A Realizable Reynolds Stress Algebraic Equation Model", NASA TM - 105993.
- StarCD_es-ice User Guides, 2008. CD-adapco.
- Tindal, M.J., Williams, T.J., Aldoory, M., 1982. "The Effect of Inlet Port Design on Cylinder Gas motion in Direct Injection Diesel Engines". ASME, Flows in Internal Combustion Engines, pp. 101-111.
- Warsi, Z.V.A., 1981. "Conservation Form of the Navier-Stokes Equations in General Nonsteady Coordinates". AIAA Journal, 19, pp. 240-242.
- Wilkes, N.S. and Thompson, C.P., 1983. "An Evaluation of Higher-order Upwind Differencing for Elliptic Flow Problems", CSS 137, AERE, Harwell.

9. RESPONSIBILITY NOTICE

The authors are the only responsible for the printed material included in this paper.